Journal of Power Sources 189 (2009) 1066–1073

Contents lists available at ScienceDirect

Journal of Power Sources

journal homepage: www.elsevier.com/locate/jpowsour

An analytical model and parametric study of electrical contact resistance in proton exchange membrane fuel cells

Zhiliang Wu [a], Shuxin Wang [a], Lianhong Zhang [a], S. Jack Hu [b,*]

[a] School of Mechanical Engineering, Tianjin University, Tianjin 300072, PR China
[b] Department of Mechanical Engineering, The University of Michigan, Ann Arbor, MI 48109-2125, USA

ARTICLE INFO

Article history:
Received 11 November 2008
Received in revised form
25 December 2008
Accepted 30 December 2008
Available online 14 January 2009

Keywords:
Electrical contact resistance
PEM fuel cell
Probability distribution

ABSTRACT

This paper presents an analytical model of the electrical contact resistance between the carbon paper gas diffusion layers (GDLs) and the graphite bipolar plates (BPPs) in a proton exchange membrane (PEM) fuel cell. The model is developed based on the classical statistical contact theory for a PEM fuel cell, using the same probability distributions of the GDL structure and BPP surface profile as previously described in Wu et al. [Z. Wu, Y. Zhou, G. Lin, S. Wang, S.J. Hu, J. Power Sources 182 (2008) 265–269] and Zhou et al. [Y. Zhou, G. Lin, A.J. Shih, S.J. Hu, J. Power Sources 163 (2007) 777–783]. Results show that estimates of the contact resistance compare favorably with experimental data by Zhou et al. [Y. Zhou, G. Lin, A.J. Shih, S.J. Hu, J. Power Sources 163 (2007) 777–783]. Factors affecting the contact behavior are systematically studied using the analytical model, including the material properties of the two contact bodies and factors arising from the manufacturing processes. The transverse Young's modulus of chopped carbon fibers in the GDL and the surface profile of the BPP are found to be significant to the contact resistance. The factor study also sheds light on the manufacturing requirements of carbon fiber GDLs for a better contact performance in PEM fuel cells.

1. Introduction

Fuel cells are receiving increasing attention as a clean power source. Among the commercially available fuel cells, proton exchange membrane (PEM) fuel cells are attractive because of their low operation temperature and quick startup. However, various irreversible losses existing in an operational PEM fuel cell tend to affect its performance and result in power losses. As part of the ohmic losses which dominate in the normal fuel cell operation, the contact resistance in PEM fuel cells has been reported to be as important as the ionic resistance [3,4]. The contact resistance also causes in-plane current non-uniformity between bipolar plate (BPP) gas channels and land areas [5,6], which may impact MEA durability and cell lifetime.

Various researchers have contributed to the prediction of the contact resistance between gas diffusion layers (GDLs) and bipolar plates (BPPs), which is a primary source of the contact resistance in PEM fuel cells [1–4,7–11]. Predictions of the contact resistance at the GDL/BPP interface in PEM fuel cells were first performed by Mishra et al. [9]. A fractal asperity based model was used to estimate the contact resistance for several GDL materials under a combination of pressure, material properties, and contact surface geometry. However, since GDLs are fundamentally porous materials, their surface characteristics may not be properly captured using commonly used surface profilometric measurement systems. Zhang et al. [10] proposed two semi-empirical methods to obtain the contact resistance versus pressure relationship with carbon papers as the GDL. One prerequisite of the semi-empirical methods is the constitutive contact resistance obtained by repeated experiments. Zhou et al. [2] numerically described the micro-contacts between the carbon fibers in a carbon paper GDL and the asperities on a graphite BPP surface. Their work was extended by Wu et al. [1] by taking into account the bending behavior and the anisotropic property of the carbon fibers using finite element method (FEM). Lai et al. [11] developed a mechanical–electrical FE model for contact resistance prediction. Although favorable agreements have been achieved in all the above-mentioned models, factors affecting the contact resistance have not been systematically studied to provide the physical insights since such parameter studies cannot be cost effectively carried out using the numerical models or experiments.

In this paper, an analytical model based on the classical statistical contact mechanics is developed for the electrical contact resistance at the interface of carbon paper GDL and graphite BPP. The contact resistance and the pressure at the interface are formulated as functions of variables that characterize the surface profiles. Probability distributions of the variables are extracted from a numerically generated GDL structure and an experimentally measured BPP surface. Two models, a simplified model and a

* Corresponding author. Tel.: +1 734 615 4315; fax: +1 734 647 7303.
E-mail address: jackhu@umich.edu (S.J. Hu).

0378-7753/$ – see front matter © 2009 Elsevier B.V. All rights reserved.
doi:10.1016/j.jpowsour.2008.12.129

generalized model, are derived to evaluate the contact resistance. In the simplified model, the micro-contact between carbon fibers in the GDL and BPP asperities is described without taking into account bending behaviors of the carbon fibers; while the generalized model presents a more general contact situation by including the bending element. Contact resistance estimates from the models are compared with experiments by Zhou et al. [2]. This analytical expression of the statistical contact also enables a parametric study to provide useful information for a good contact performance in PEM fuel cells.

2. Contact resistance model

The contact at the GDL/BPP interface actually happens as micro-contacts between GDL carbon fibers and BPP surface asperities. The contact responses at the interface, including contact force and electrical contact resistance, are the overall effect of all the micro-contacts with each micro-contact spot contributing a certain contact force and resistance to the current flow across the interface. The force over the nominal contact area is equivalent to the sum of the contact forces on all individual micro-contacts. The total contact resistance is composed of a series of resistances from the micro-contact spots in parallel.

Using the probability theory, the pressure over the nominal contact area can be expressed as:

$$P = \frac{N_a}{A_n} \underbrace{\int\int \cdots \int_m} F_c(x_1, x_2, \ldots, x_m) f(x_1, x_2, \ldots, x_m) \, dx_1 \, dx_2 \ldots dx_m \quad (1)$$

where F_c is the contact force on each micro-contact spot, $f(x_1, x_2, \ldots, x_m)$ is the joint probability density function of the random variables x_i ($i = 1, 2, \ldots, m$) that influence the contact force, A_n is the nominal contact area, and N_a is the number of BPP asperities at the interface.

Similarly, the contact resistance can be expressed as:

$$R = \frac{A_n}{N_a} \left[\underbrace{\int\int \cdots \int_k} \frac{r(y_1, y_2, \ldots, y_k)}{R_c(y_1, y_2, \ldots, y_k)} \, dy_1 \, dy_2 \ldots dy_k \right]^{-1} \quad (2)$$

where R_c is the contact resistance on each micro-contact spot, $r(y_1, y_2, \ldots, y_k)$ is the joint probability density function of the random variables y_j ($j = 1, 2, \ldots, k$) that influence the contact resistance.

Hence, the relationship between the contact resistance and the pressure (P–R relationship in short) can be written as:

$$P \cdot R = \frac{\underbrace{\int\int \cdots \int_m} F_c(x_1, x_2, \ldots, x_m) f(x_1, x_2, \ldots, x_m) \, dx_1 \, dx_2 \ldots dx_m}{\underbrace{\int\int \cdots \int_k} \frac{r(y_1, y_2, \ldots, y_k)}{R_c(y_1, y_2, \ldots, y_k)} \, dy_1 \, dy_2 \ldots dy_k} \quad (3)$$

Eq. (3) can be solved using the following procedure:

(1) Determine the micro-contact pair at the GDL/BPP interface. The contact resistance at the interface was reported to be governed by micro-contacts between carbon fibers in the carbon paper and graphite asperities on the BPP surface [2]. Thus, the contact bodies under investigation are carbon fibers and graphite asperities.
(2) Formulate the contact force and the contact resistance for micro-contacts. Since current polymer-graphite bipolar plates are relatively brittle and carbon fibers are also commonly known as brittle fibers, only elastic deformation needs to be considered.
(3) Determine the joint probability density functions $f(x_1, x_2, \ldots, x_m)$ and $r(y_1, y_2, \ldots, y_k)$.
(4) Calculate by Eqs. (1) and (2) the contact resistance over the GDL/BPP interface at different pressures and obtain the P–R relationship.

The following assumptions are made in the calculation within the loading range: (1) each micro-contact is far enough from the others so that interaction effect among the contacts is negligible; (2) no large strain deformation occurs for both the BPP and the GDL; (3) the micro-contact surfaces are perfectly smooth; (4) frictional forces at the micro-contacts are negligible; and (5) the micro-contact area is planar and circular. The last assumption ensures that the contact resistance at individual micro-contact can be described using Holm's equation [12]:

$$R_c = \frac{\rho_1 + \rho_2}{4\sqrt{A_c/\pi}} \quad (4)$$

where A_c is the micro-contact area, ρ_1 and ρ_2 are the resistivities of the two contact bodies.

2.1. Simplified contact resistance model

The micro-contact between a BPP asperity and a carbon fiber can be modeled as a hemisphere in contact with an external cylinder using the Greenwood–Williamson (GW) model for rough surfaces [13]. When the micro-contact model is developed without considering the bending behaviors of the carbon fibers, the model can be simplified as a hemisphere in contact with a fixed cylinder, as shown in Fig. 1. The relationship between an elastic displacement δ and a compressive load F_c can be obtained using the Hertz theory [14] as:

$$F_c = \frac{4}{(3E^* R_e^{1/2} \delta^{3/2})} \quad (5)$$

and the contact area is given by:

$$A_c = \pi R_e \delta \quad (6)$$

where R_e is the equivalent radius, $R_e = R_1\sqrt{R_2/(R_1 + R_2)}$, R_1 and R_2 are the radii of the BPP asperity and the carbon fiber respectively; and E^* is the equivalent elastic modulus as $E^* = 1/((1 - \nu_1^2/E_1) + (1 - \nu_{2T}^2/E_{2T}))$, E_1, E_{2T}, ν_1, ν_{2T} are Young's moduli and Poisson's ratios of the BPP asperity and the carbon fiber respectively. The subscription T indicates the transverse direction. By substituting Eq. (6) into Eq. (4), the contact resistance is obtained as:

$$R_c = \frac{\rho_1 + \rho_2}{4\sqrt{R_e \delta}} \quad (7)$$

An estimate of the number of asperities on the BPP surface, N_a, can be approximated as:

$$N_a = D_{sum} A_n \quad (8)$$

where D_{sum} is the density of the BPP summits, which can be obtained by experimental profilometric measurement of the surface.

As illustrated in Fig. 1(b), when the separation between the summit mean plane of the BPP and the envelop surface of the GDL, d, is specified, the elastic displacement δ can be readily obtained as a function of the horizontal distance s and the asperity height h. By substituting Eqs. (5)–(8) into Eqs. (1) and (2), the pressure and the contact resistance over the nominal contact area are reduced to:

$$P = C_P \iint \left[\delta(h, s)\right]^{3/2} \cos\theta(h, s) f(h, s) \, dh \, ds \quad (9)$$

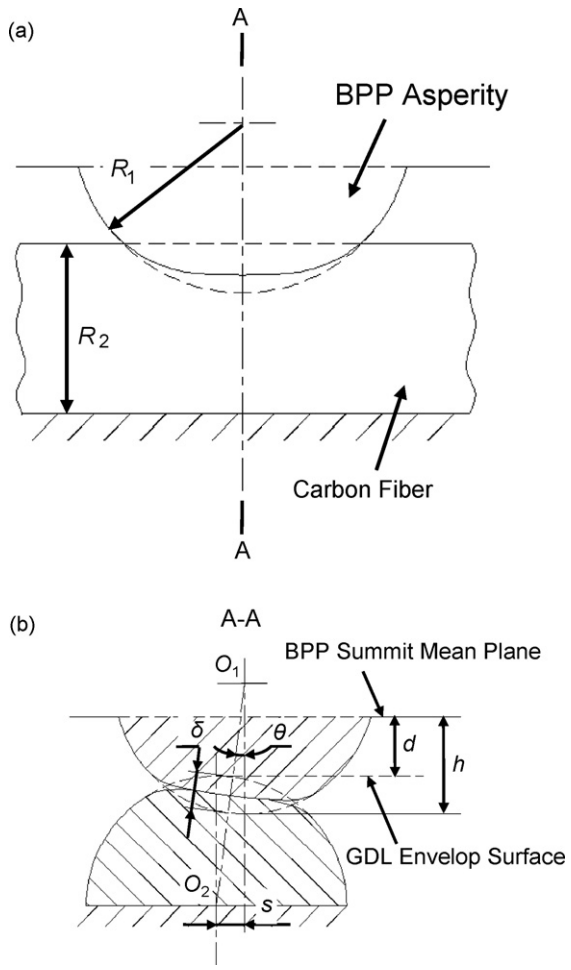

Fig. 1. Schematic of the simplified contact model: δ is the elastic displacement; h is the asperity height; and d is the separation between the summit mean plane of the BPP and the envelope surface of the GDL.

$$R = C_R\left\{\iint \left[\delta(h,s)\right]^{1/2} f(h,s)\,dh\,ds\right\}^{-1} \tag{10}$$

where $C_P = (4E^*D_{sum}R_e^{1/2})/3$ and $C_R = (\rho_1+\rho_2)/(4D_{sum}R_e^{1/2})$. The probability density functions $f(h,s)$ and $r(h,s)$ can be factorized in terms of the product of the marginal density functions of h and s since the two variables are independent. Eqs. (9) and (10) are expressed accordingly as:

$$P = C_P \iint \left[\delta(h,s)\right]^{3/2} \cos\theta(h,s) f_H(h) f_S(s)\,dh\,ds \tag{11}$$

$$R = C_R\left\{\iint \left[\delta(h,s)\right]^{1/2} f_H(h) f_S(s)\,dh\,ds\right\}^{-1} \tag{12}$$

2.2. Generalized contact resistance model

The simplified model will not be sufficient for micro-contacts when the load on BPP asperities causes bending in the carbon fibers because such bending would alter the contact responses. In this section, a generalized micro-contact model is developed as a hemisphere in contact with a simply supported beam. The schematic of the model is shown in Fig. 2.

Fig. 2 indicates that the contact responses by the generalized model are closely related to the length of the carbon fiber, the contact location, and the transverse displacement. The transverse

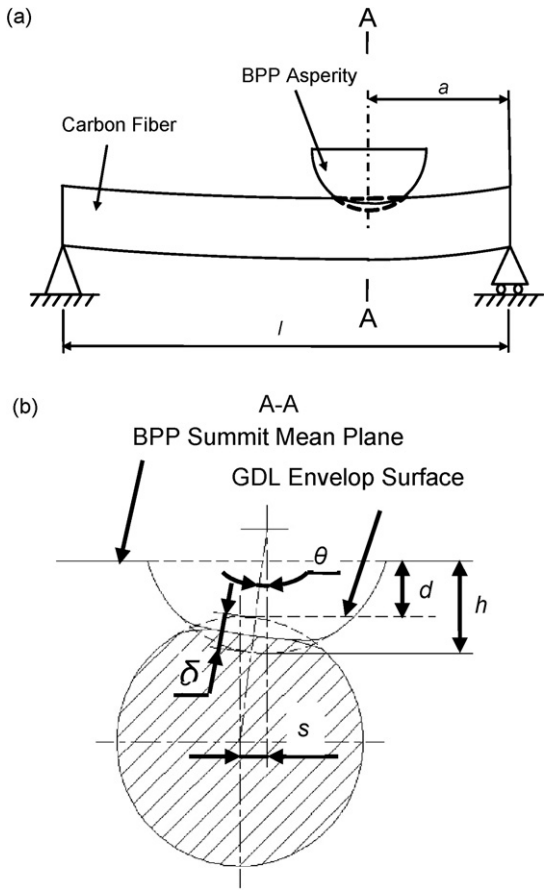

Fig. 2. Schematic of the generalized contact model between a BPP asperity and a carbon fiber: l is the length of the carbon fiber; $a = l{\cdot}t(0 \le t \le 0.5)$ denotes the contact location, which is the longitudinal distance from the center of the asperity to the nearer end of the carbon fiber; and δ is the transverse displacement.

displacement consists of the fiber deflection and the elastic displacement as:

$$\delta = \delta_d + \delta_c = \frac{\left[F_c(0.25-t^2)^2 l^3\right]}{(3E_{2L}I) + \left[(3F_c)/\left(4E^*R_e^{1/2}\right)\right]^{2/3}} \tag{13}$$

where δ_d denotes the fiber deflection, δ_c denotes the elastic displacement, E_{2L} and I are the longitudinal Young's modulus and the moment of inertia of the carbon fiber. The transverse displacement δ in Eq. (13) can be similarly obtained as a function of the asperity height and the horizontal distance as in the simplified model. The micro-contact force can then be determined by solving the following cubic equation [15]:

$$x^3 + c_2x^2 + c_0 = 0 \tag{14}$$

where

$$x = F_c^{1/3},$$

$$c_2 = \frac{(3^{5/3}E_{2L}I)}{[(4E^*)^{2/3}(0.25-t^2)^2 l^3 R_e^{1/3}]},$$

and

$$c_0 = -\frac{(3E_{2L}I\delta)}{[(0.25-t^2)^2 l^3]}.$$

Due to the coupling effect between the fiber deflection and the elastic displacement, there exists an error in the solution of the

contact force by Eq. (14). Such error can be corrected by applying a coefficient that estimates the deviation of the prediction from the results by the finite element method (FEM). The coefficient is obtained by the following regression model:

$$err = 1.42 - 0.00204l - 0.0303a - 0.155\delta + 0.000227a^2 + 0.0587\delta^2 + 0.000303la - 0.00564a\delta \quad (15)$$

where a is a variable denoting the contact location in the horizontal direction, as shown in Fig. 2. Eq. (15) is found to be significant ($p < 0.0005$) and with an adjusted R-square 97.2%. The resulted contact force is modified as:

$$F_c' = err \cdot F_c \quad (16)$$

The contact resistance is given as:

$$R_c = \frac{\rho_1 + \rho_2}{4\sqrt{R_e \delta_c}} \quad (17)$$

It is apparent from Eqs. (13) and (17) that the contact responses by the generalized model are functions of independent random variables that include length of the carbon fiber section l, contact location parameter t, BPP asperity height h, and horizontal distance s. The pressure and the contact resistance over the nominal contact area are then formulated as:

$$P = D_{sum} \int\int\int\int F_c'(l, t, h, s) \cos\theta(h, s) f_L(l) f_T(t) f_H(h) f_S(s)\, dl\, dt\, dh\, ds \quad (18)$$

$$R = \frac{\rho_1 + \rho_2}{4 D_{sum} {R_e}^{1/2}} \times \left[\int\int\int\int \left[\delta_c(l, t, h, s)\right]^{1/2} f_L(l) f_T(t) f_H(h) f_S(s)\, dl\, dt\, dh\, ds\right]^{-1} \quad (19)$$

2.3. Probability density functions of random variables

For both the simplified and the generalized models, the probability density functions of random variables l, t, h, and s are extracted from the numerical models by Wu et al. [1] and Zhou et al. [2], where the GDL structure is built in accordance with the wet-laid papermaking process for carbon papers [16] and the BPP surface is established as a regular engineering surface with the GW model [13]. The BPP surface model is generated from experimental measurements of a grade FU 4369 graphite plate from PEM Technology Inc. and the GDL structure is developed using the technical data of a Toray TGP-H-30 carbon paper. The probability density functions $f_L(l)$, $f_T(t)$, $f_H(h)$, and $f_s(s)$ are determined as:

$$f_L(l) = \frac{1}{27} \exp\left(-\frac{l}{27}\right), \quad l > 0 \quad (20)$$

$$f_T(t) = 2, \quad 0 < t < 0.5 \quad (21)$$

$$f_H(h) = \frac{1}{3.55\sqrt{2\pi}} \exp\left[-\frac{h^2}{2 \times 3.55^2}\right], \quad -\infty < h < \infty \quad (22)$$

$$f_S(s) = \frac{1}{5} \exp\left(-\frac{s}{5}\right), \quad s > 0 \quad (23)$$

That is, BPP asperity height h has a normal distribution with a mean of zero and a variance of 3.55^2 μm^2; length of the carbon fiber section l follows an exponential distribution with a mean of 27 μm; contact location parameter t is uniformly distributed between 0 and 0.5; and horizontal distance s also follows an exponential distribution with a mean of 5 μm.

Table 1
Parameters for the contact surface profiles [2].

Parameters	Value
BPP summit radius R_1 (μm)	3.67
BPP summit density D_{sum} (#mm^{-2})	98[2]
GDL carbon fiber length density (mm mm^{-2})	57
GDL carbon fiber radius R_2 (μm)	3.5

Table 2
Material properties of BPP asperities and carbon fibers.

Properties	BPP asperity	Carbon fiber
Young's modulus E_L (GPa)	10[a]	230[b]
Transverse Young's modulus E_T (GPa)		3.2[a]
Poisson's ratio ν_{LT}	0.26[a]	0.256[c]
Transverse Poisson's ratio ν_{TT}		0.3[c]
Electrical resistivity ρ (μΩ m)	190[a]	70[a]

[a] Reported by Ref. [2].
[b] Reported by Ref. [17].
[c] Reported by Ref. [18].

Parameters for the BPP surface profile and the GDL structure are listed in Table 1. Material properties of the BPP asperities and the carbon fibers are listed in Table 2.

3. Results and discussion

3.1. Contact resistance predictions

The P–R relationship is estimated by the simplified and generalized models for the contact between a Toray TGP-H-30 carbon paper and a grade FU 4369 graphite plate. Reasonable agreements are observed with the experimental data by Zhou et al. [2], as shown in Fig. 3. The similarity in results from the two models in the figure indicates that the P–R relationship can be estimated with an adequate accuracy by the simplified model for contact situations when the carbon paper GDL bears a fiber length density similar to that of TGP-H-30 carbon papers. For such contact situations, the elastic displacement accounts for a large part of the overall transverse displacement and the bending behavior of the carbon fiber can be neglected. This is because the length of the carbon fiber section in contact decreases as the fiber length density in the GDL grows. When the fiber length density in the GDL is sufficiently high, the carbon fiber section in contact is short and the transverse deflection at

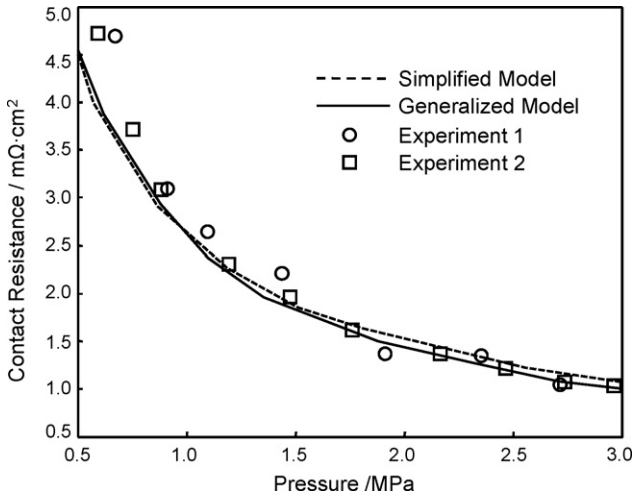

Fig. 3. The estimated P–R relationship of contact resistance vs. pressure by the simplified and generalized analytical models: a Toray TGP-H-30 carbon paper and a grade FU 4369 graphite plate are used as the GDL and the BPP respectively.

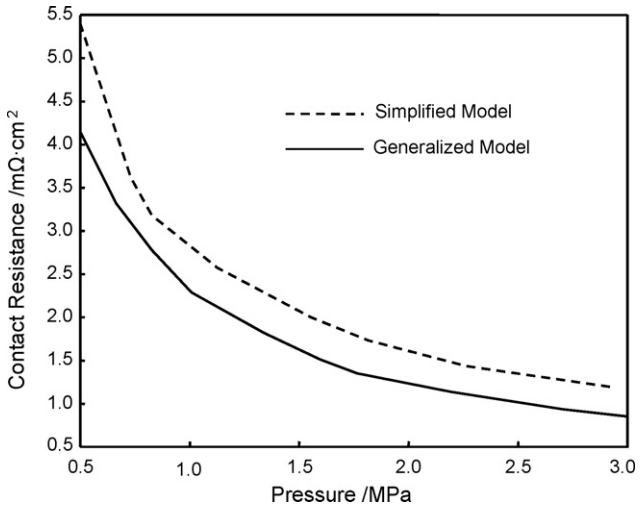

Fig. 4. The estimated *P–R* relationship by the simplified and generalized models with a fiber length density of 36 mm mm^{-2}.

individual contact location is small enough to be neglected. Therefore, under the assumption of no large strain for the two contact bodies, estimates of the contact resistance provided by the simplified model may be comparable to those by the generalized model. On the contrary, when the fiber length density in the GDL is low, the slenderness ratio of carbon fiber sections in contact becomes large and the transverse deflection at the contact locations would be of the same level or even larger than the elastic displacement. In this case, the simplified model is no longer sufficient, as shown in Fig. 4, where a large deviation from the estimates by the generalized model is observed.

Accuracy of the generalized model depends on feasible formulae of the micro-contact responses and correct determination of the probability distribution of random variables in effect. The analytical result of the contact force is corrected by a regression coefficient calculated by Eq. (15). The error introduced by statistical approximation can be identified by comparing the analytical result with a numerical result obtained by summing individual micro-contact responses. Both models use Eqs. (14)–(18) to calculate the micro-contact responses, but differ in the calculation of the overall contact force and contact resistance at the GDL/BPP interface. The minor difference between the two curves in Fig. 5 confirms the probability density functions of the random variables in the analytical

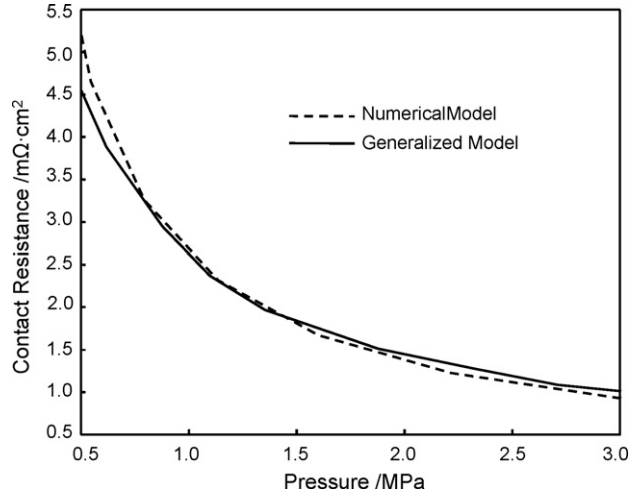

Fig. 5. Comparison between the generalized model and a numerical simulation.

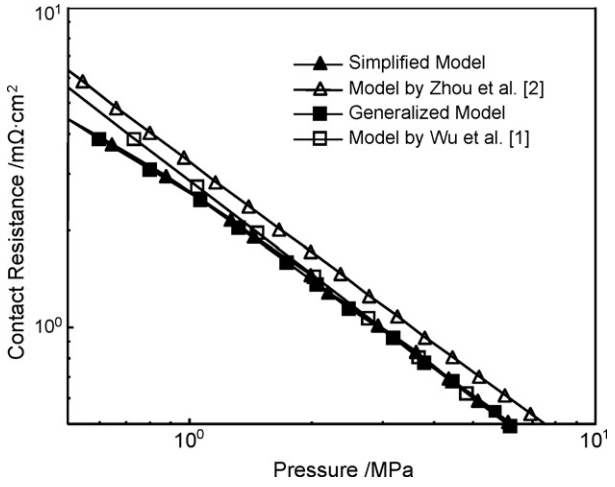

Fig. 6. Comparisons between the simplified model and the model by Zhou et al. [2] and between the generalized model and the model by Wu et al. [1].

model. The comparatively large difference between the two results at low pressure can be attributed to a relatively small number of micro-contact spots at such pressures. Insufficient sample points at low pressure induce biases on the estimates of expectations of the micro-contact force and micro-contact resistance. Such biases eventually cause a deviation from the actual contact situation. Comparisons between the simplified model and the numerical model by Zhou et al. [2] and between the generalized model and the numerical model by Wu et al. [1] also indicate the biases at low pressures, as shown in Fig. 6.

3.2. Parametric study

One distinct feature of the generalized model is the analytical expressions of the contact responses, which facilitate a systematic investigation on the effects of material properties of the two contact bodies and their manufacturing processes.

Parameters regarding the BPP surface profile include asperity density, asperity radius, and standard deviation of asperity height. Effects of these three parameters on the contact resistance are shown in Figs. 7–9 respectively. Fig. 7 indicates that an increase in BPP asperity density would induce a decrease in the contact

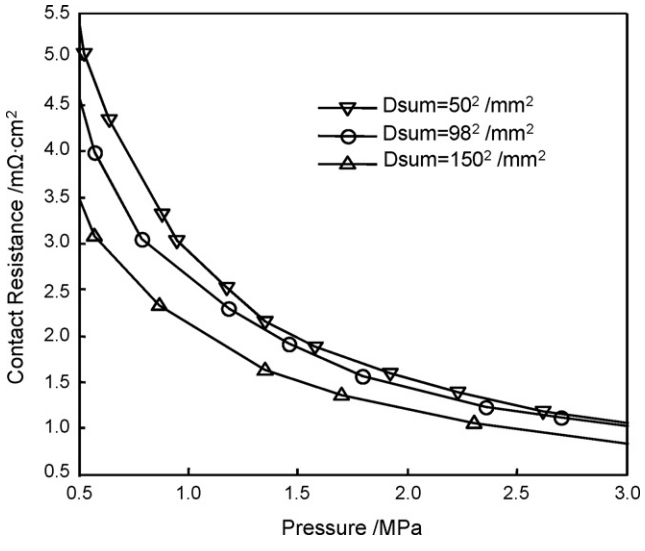

Fig. 7. The *P–R* relationships for different BPP asperity densities.

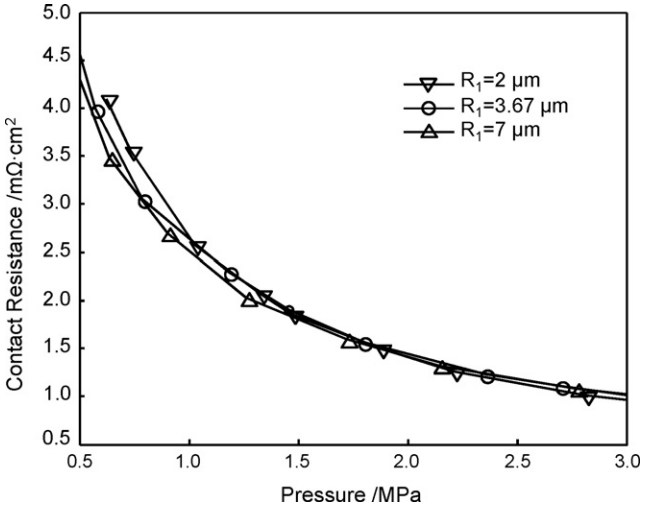

Fig. 8. The *P–R* relationships for different BPP asperity radii.

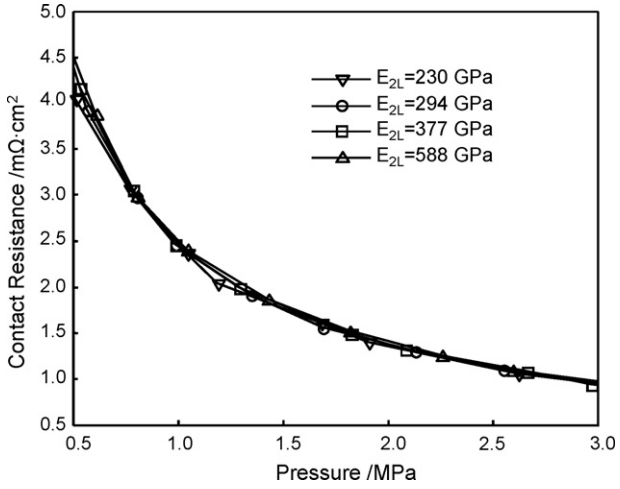

Fig. 10. The *P–R* relationships for different longitudinal Young's moduli of chopped carbon fibers: the moduli are selected from technical data of Toray PAN-based carbon fibers [19].

resistance. The increase in asperity density increases the number of micro-contacts but reduces the average micro-contact area at the GDL/BPP interface. The growth in the number of micro-contacts decreases the contact resistance, while the reduction in the micro-contact area increases the contact resistance. The change in the contact resistance, as shown in Fig. 7, is more significant with the change of the number of micro-contacts than with the change of the micro-contact area. For various BPP surface profiles with different asperity radii, the contact resistance at the interface tends to decrease as the radius increases. Under a contact situation with a certain transverse displacement, the BPP surface profile with a larger asperity radius is associated with a higher pressure at the interface. Hence, compared at the same pressure, the surface profile with a larger asperity radius has a smaller transverse displacement, a smaller number of micro-contacts, but a larger average micro-contact force. The change of the contact resistance at the interface is finally determined by the changes in the number of micro-contacts and the micro-contact area, as indicated in Fig. 8. Comparison in Fig. 9 shows that variation of BPP asperity height may significantly affect the contact resistance. With a smaller variation, the cell may exhibit a better performance regarding the contact resistance: a lower contact resistance can be achieved and the contact resistance decreases more quickly to a steady state.

Material properties of chopped carbon fibers in carbon paper GDLs are also significant to the contact resistance at the GDL/BPP interface. Factors of concern are Young's modulus, fiber radius, and fiber section length. The chopped carbon fibers bear typical anisotropic properties. The longitudinal Young's modulus is usually an order of magnitude higher than the transverse modulus. When a BPP asperity comes into contact with a carbon fiber, deflection of the carbon fiber depends on the longitudinal Young's modulus, while the elastic displacement is determined by the transverse modulus. Effects of the longitudinal and transverse Young's moduli on the contact resistance are shown in Figs. 10 and 11 respectively. In Fig. 10, no distinct deviation is observed among the *P–R* curves for standard modulus, intermediate modulus, and high modulus carbon fibers (classified as Toray carbon fibers); while as the results indicated in Fig. 11, a growth in the transverse Young's modulus causes an increase in the contact resistance. For contact situations under the same pressure, an increase in the transverse Young's modulus would cause a decrease in the number of micro-contacts and a reduction in the micro-contact area, which eventually lead to an increase in the contact resistance. Difference among the *P–R* curves in Fig. 11 indicates that using chopped carbon fibers of

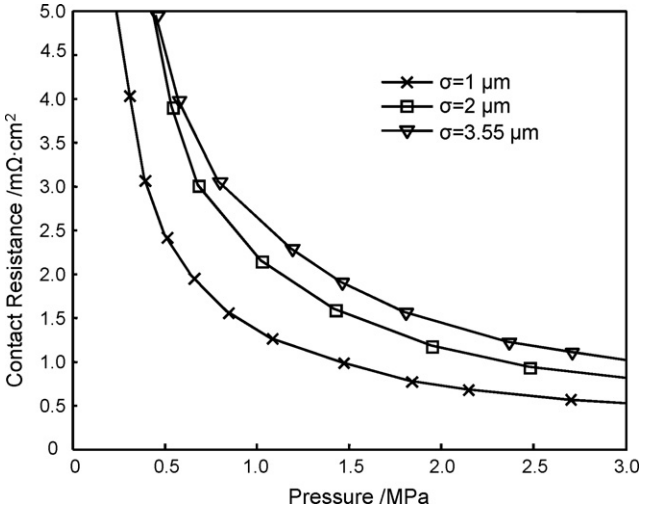

Fig. 9. The *P–R* relationships for different variations of BPP asperity height.

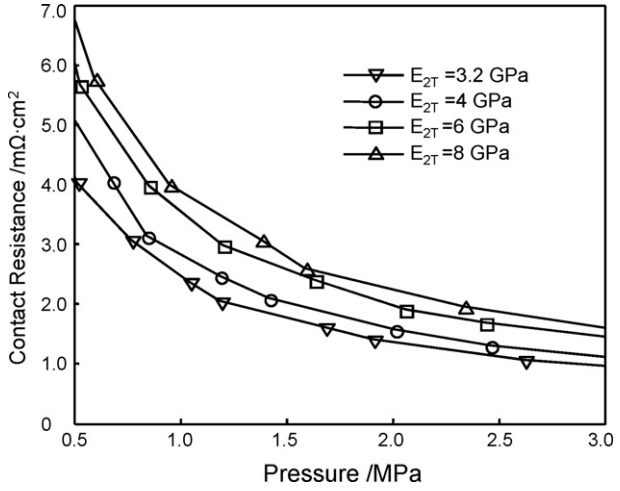

Fig. 11. The *P–R* relationships for different transverse Young's moduli of chopped carbon fibers: the moduli are selected from specific values of Toray PAN-based carbon fibers [20].

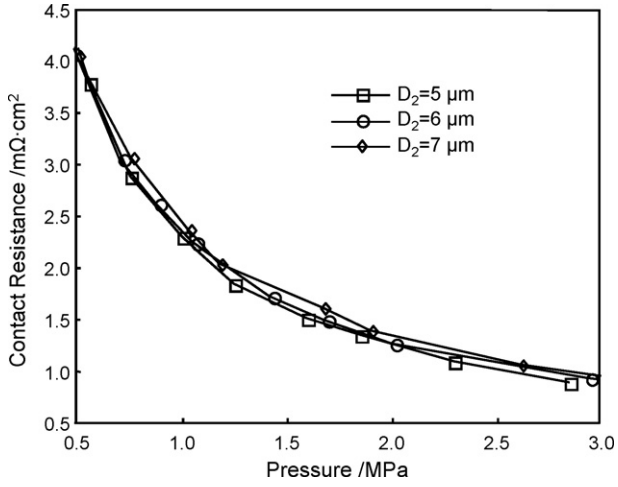

Fig. 12. The *P–R* relationships for different carbon fiber diameters: the diameters are selected from technical data of Toray PAN-based carbon fibers [19].

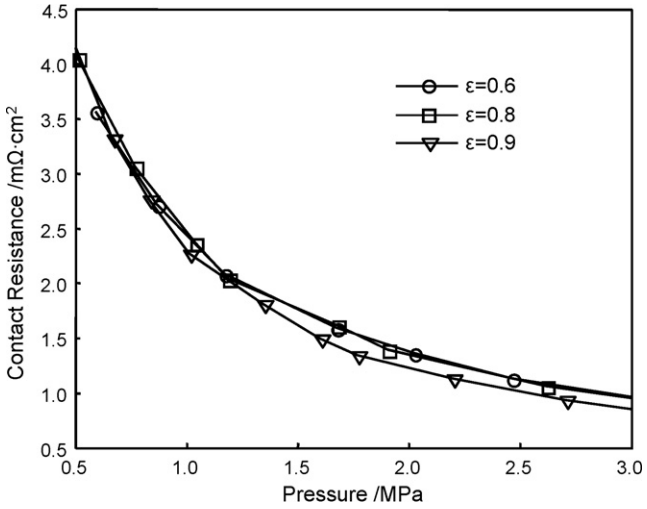

Fig. 14. The *P–R* relationships for different carbon paper porosities.

lower transverse Young's modulus can effectively reduce the contact resistance.

The typical diameter of the PAN precursor fiber is about 15 μm, which ultimately results in a carbon fiber with a diameter of about 7 μm [21]. The impact of carbon fiber diameter on the *P–R* relationship is illustrated in Fig. 12, where a favorable reduction in the contact resistance occurs when the fiber diameter decreases from 7 to 5 μm. However, current fiber-production technology makes it difficult and expensive to process a PAN fiber with a diameter significantly less than 15 μm [21]. Using a carbon fiber with a diameter of less than 7 μm may result in worse cost-performance of PEM fuel cells. Carbon fibers in carbon papers are usually chopped into a fixed length. If the length is too short, strength and handling properties of the carbon paper may be reduced. On the other hand, if the length is too long, dispersion irregularities may occur, causing in local regions a lower porosity that causes potential damage to the carbon paper or localized thinning of the membrane or catalyst layer in PEM fuel cells when pressure is applied [22]. Fig. 13 compares the *P–R* relationships for chopped carbon fibers with different lengths. Result shows that using shorter carbon fibers may improve the contact performance with a smaller contact resistance, especially at lower pressures. Therefore, carbon fibers with a shorter length could be a premier option when requirements of strength, handling properties, and uniform dispersion are met.

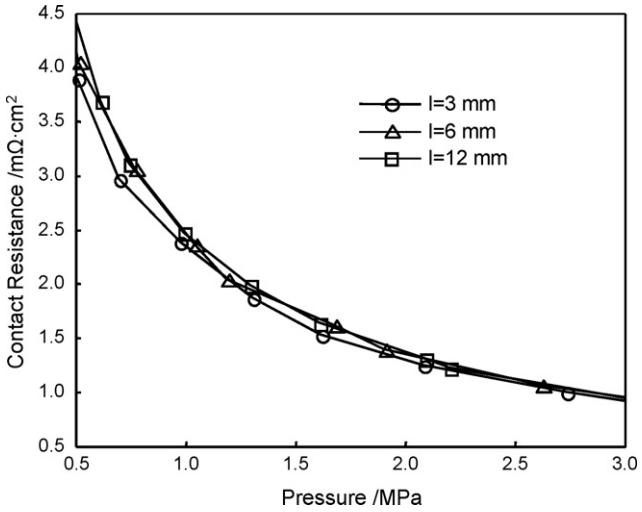

Fig. 13. The *P–R* relationships for different carbon fiber lengths, in which 6 mm is regarded as a preferable length in Ref. [22].

Porosity is one critical parameter that actually controls the configuration of carbon papers. Although it is not an explicit variable in the analytical model, its effect can be investigated by altering GDL fiber length density. Porosity and fiber length density are closely related since the density can be expressed as a function of the porosity as indicated in Zhou et al. [2]:

$$L_F = \frac{4(1-\varepsilon)V_{GDL}}{\pi d_F^2} \tag{24}$$

where L_F is the fiber length density, ε the porosity, V_{GDL} the volume of GDL, and d_F the fiber diameter. The fiber length density can eventually be represented by two parameters in the analytical expressions, that is, the distributions of carbon fiber section in contact and the horizontal distance. A larger porosity is associated with a lower fiber length density, which results in average a longer fiber section in contact and a larger horizontal distance. The *P–R* relationships for different porosities are illustrated in Fig. 14. Comparison shows that the contact resistance increases as the porosity decreases. As the porosity decreases, carbon fiber sections in contact become shorter, causing smaller deflection and a reduction in the number of micro-contacts, which eventually result in an increase in the contact resistance. This trend may seem inconsistent with the common belief that a better contact performance would be achieved with more carbon fibers in the carbon paper GDL. The fact is that although a GDL with a higher fiber length density tends to have more micro-contacts with BPP asperities, its deformation under the same pressure would have to be smaller, which in turn reduces the number of micro-contacts at the interface. The combination of the two effects finally determines the variation of the contact resistance. The combined effect may also explain the possible existence of an optimal value for the GDL porosity, beyond which any further reduction may not cause apparent improvement on the *P–R* curve, as comparison shown in Fig. 14 when the porosity reduces from 0.8 to 0.6.

As indicated in the analytical models of contact force and contact resistance, the probability distribution of the four random variables may also affect the *P–R* relationship. Besides the BPP asperity height, factors of concern include length of the carbon fiber section in contact and horizontal distance. Distributions of the two factors depend on the specific structure of carbon papers and can be therefore traced to the effects of carbon paper porosity and length of the chopped carbon fibers. In addition, lower resistivities of the

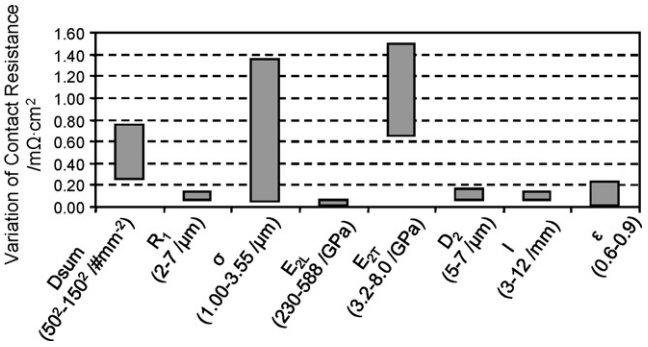

Fig. 15. Variation of contact resistance with various parameters: the pressure ranging from 1 to 3 MPa.

GDL and the BPP would result in a lower contact resistance at the interface.

3.3. Summary of parametric study results

Fig. 15 summarizes the effects of various parameters on the contact resistance. Among all the parameters regarding BPP surface profile, material property of chopped carbon fibers, and configuration of GDL, the transverse Young's modulus of chopped carbon fibers and the standard deviation of BPP asperity height are indicated as the most significant factors that affect the contact resistance at the GDL/BPP interface. A visible variation in the contact resistance can also be expected by a change in BPP asperity density. Changes in the BPP asperity radius, diameter and length of the chopped carbon fibers in the GDL cause a small variation in the contact resistance, but these parameters should also be considered with regard to the cost-performance of PEM fuel cells, material property requirement, and handling requirement.

4. Conclusions

An effective analytical model is developed in this paper to estimate the electrical contact resistance between graphite BPPs and the carbon paper GDLs in PEM fuel cells. Random variables that feature the BPP surface roughness and the GDL structure are employed to characterize the actual contact situation at the interface. Estimates of the contact resistance by the model agree well with existing experimental data. The analytical model also facilitates a systematical parametric study on factors that affect the contact responses, include material properties of the two contact bodies and factors arising from the manufacturing processes. Among all the parameters investigated, the transverse Young's modulus of chopped carbon fibers in carbon paper GDLs and BPP surface profile are found to be most significant to the contact resistance. The parametric study also sheds light on the manufacturing of carbon fiber GDLs for a better contact performance in PEM fuel cells.

Acknowledgements

The work reported here is sponsored by the Specialized Research Fund for the Doctoral Program of Higher Education of the Ministry of Education of China (Grant No. 20050056006), Cheung Kong Scholars Programs of the Ministry of Education of China and Tianjin University, and the Research Fund of The Key Laboratory of Advanced Manufacturing Technology & Equipment of Tianjin, China. The authors gratefully acknowledge these supports.

References

[1] Z. Wu, Y. Zhou, G. Lin, S. Wang, S.J. Hu, J. Power Sources 182 (2008) 265–269.
[2] Y. Zhou, G. Lin, A.J. Shih, S.J. Hu, J. Power Sources 163 (2007) 777–783.
[3] H.A. Gasteiger, W. Gu, R. Makharia, M.F. Mathias, B. Sompalli, in: W. Vielstich, A. Lamm, H.A. Gasteiger (Eds.), Handbook of Fuel Cells: Fundamentals, Technology, and Applications, V3: Fuel Cell Technology and Application, Wiley, 2003, pp. 593–610.
[4] F. Barbir, J. Braun, J. Neutzler, J. New Mat. Electrochem. Syst. 2 (1999) 197–200.
[5] H. Meng, C.Y. Wang, J. Electrochem. Soc. 151 (2004) A358–A367.
[6] J. Li, C.Y. Wang, A. Su, J. Electrochem. Soc. 155 (2008) B64–B69.
[7] T. Berning, N. Djilali, J. Power Sources 124 (2003) 440–452.
[8] J. Ihonen, M. Mikkola, G. Lindbergh, J. Electrochem. Soc. 151 (2004) A1152–A1161.
[9] V. Mishra, F. Yang, R. Pitchumani, J. Fuel Cell Sci. Technol. 1 (2004) 2–9.
[10] L. Zhang, Y. Liu, H. Song, S. Wang, Y. Zhou, S.J. Hu, J. Power Sources 162 (2006) 1165–1171.
[11] X. Lai, D. Liu, L. Peng, J. Ni, J. Power Sources 182 (2008) 153–159.
[12] R. Holm, Electric Contacts Theory and Application, Springer-Verlag, New York, 1967, pp. 9–16.
[13] J.A. Greenwood, J.B.P. Williamson, Proc. R. Soc. Lond. A295 (1966) 300–319.
[14] K.L. Johnson, Contact Mechanics, Cambridge University Press, 1985, pp. 84–106.
[15] Wolfram Mathworld, http://mathworld.wolfram.com/CubicFormula.html.
[16] M.F. Mathias, J. Roth, J. Fleming, W. Lehnert, in: W. Vielstich, A. Lamm, H.A. Gastegier (Eds.), Handbook of Fuel Cells, Fundamentals, Technology and Applications, Vol. 3, Fuel Cell Technology and Applications., John Wiley & Sons, Ltd., New York, 2003, pp. 517–537.
[17] Toray, Toray Carbon Fiber Paper "TGP-H".
[18] H. Miyagawa, c. Sato, T. Mase, E. Drown, L.T. Drzal, K. Ikegami, Mater. Sci. Eng. A 412 (2005) 88–92.
[19] Toray Carbon Fibers America, Inc., Technical data sheet.
[20] P. Morgan, Carbon Fiber and Their Composites, Taylor & Francis, Boca Raton, 2005, pp. 814.
[21] M.L. Minus, S. Kumar, JOM 57 (2005) 52–58.
[22] M. Inoue, U.S. Patent, 6,489,051 (1999).